H_0 from ten well-measured time delay lenses

S. Rathna Kumar[1,2], C. S. Stalin[1], and T. P. Prabhu[1]

[1] Indian Institute of Astrophysics, II Block, Koramangala, 560 034 Bangalore, India
   e-mail: rathna@iiap.res.in
[2] Physical Research Laboratory, Navrangpura, 380 009 Ahmedabad, India

ABSTRACT

In this work, we present a homogeneous curve-shifting analysis using the difference-smoothing technique of the publicly available light curves of 24 gravitationally lensed quasars, for which time delays have been reported in the literature. The uncertainty of each measured time delay was estimated using realistic simulated light curves. The recipe for generating such simulated light curves with known time delays in a plausible range around the measured time delay is introduced here. We identified 14 gravitationally lensed quasars that have light curves of sufficiently good quality to enable the measurement of at least one time delay between the images, adjacent to each other in terms of arrival-time order, to a precision of better than 20% (including systematic errors). We modeled the mass distribution of ten of those systems that have known lens redshifts, accurate astrometric data, and sufficiently simple mass distribution, using the publicly available PixeLens code to infer a value of H_0 of 68.1 ± 5.9 km s^{-1} Mpc^{-1} (1σ uncertainty, 8.7% precision) for a spatially flat universe having $\Omega_m = 0.3$ and $\Omega_\Lambda = 0.7$. We note here that the lens modeling approach followed in this work is a relatively simple one and does not account for subtle systematics such as those resulting from line-of-sight effects and hence our H_0 estimate should be considered as indicative.

Key words. gravitational lensing: strong – methods: numerical – cosmological parameters – quasars: general

1. Introduction

The Hubble constant at the present epoch (H_0), the current expansion rate of the universe, is an important cosmological parameter. All extragalactic distances, as well as the age and size of the universe depend on H_0. It is also an important parameter in constraining the dark energy equation of state and it is used as input in many cosmological simulations (Freedman & Madore 2010; Planck Collaboration XVI 2014). Therefore, precise estimation of H_0 is of utmost importance in cosmology.

Estimates of H_0 available in the literature cover a wide range of uncertainties from ∼2% to ∼10% and the value ranges between 60 and 75 km s^{-1} Mpc^{-1}. The most reliable measurements of H_0 known to date include

- the *Hubble* Space Telescope (HST) Key Project (72 ± 8 km s^{-1} Mpc^{-1}; Freedman et al. 2001),
- the HST Program for the Luminosity Calibration of Type Ia Supernovae by Means of Cepheids (62.3 ± 5.2 km s^{-1} Mpc^{-1}; Sandage et al. 2006),
- *Wilkinson* Microwave Anisotropy Probe (WMAP) (70.0 ± 2.2 km s^{-1} Mpc^{-1}; Hinshaw et al. 2013),
- Supernovae and H_0 for the Equation of State (SH0ES) Program (73.8 ± 2.4 km s^{-1} Mpc^{-1}; Riess et al. 2011),
- Carnegie Hubble Program (CHP) (74.3 ± 2.6 km s^{-1} Mpc^{-1}; Freedman et al. 2012),
- the Megamaser Cosmology Project (MCP) (68.9 ± 7.1 km s^{-1} Mpc^{-1}; Reid et al. 2013; Braatz et al. 2013),
- *Planck* measurements of the cosmic microwave background (CMB) anisotropies (67.3 ± 1.2 km s^{-1} Mpc^{-1}; Planck Collaboration XVI 2014), and
- Strong lensing time delays ($75.2^{+4.4}_{-4.2}$ km s^{-1} Mpc^{-1}; Suyu et al. 2013).

It is worth noting here that the small uncertainties in H_0 measurements resulting from WMAP and *Planck* crucially depend on the assumption of a spatially flat universe.

Although the values of H_0 obtained from different methods are consistent with each other within 2σ given the current level of precision, all of the above methods of determination of H_0 suffer from systematic uncertainties. Therefore, as the measurements increase in precision, multiple approaches based on different physical principles need to be pursued so as to be able to identify unknown systematic errors present in any given approach.

The phenomenon of strong gravitational lensing offers an elegant method to measure H_0. For gravitationally lensed sources that show variations in flux with time, such as quasars, it is possible to measure the time delay between the various images of the background source. The time delay, which is a result of the travel times for photons being different along the light paths corresponding to the lensed images, has two origins: (i) the geometric difference between the light paths and (ii) gravitational delay due to the dilation of time as photons pass in the vicinity of the lensing mass. Time delays, therefore depend on the cosmology, through the distances between the objects involved, and on the radial mass profile of the lensing galaxies. This was shown theoretically five decades ago by Refsdal (1964) long before the discovery of the first gravitational lens Q0957+561 by Walsh et al. (1979).

Estimation of H_0 through gravitational lens time delays, although it has its own degeneracies, is based on the well-understood physics of General Relativity, and compared to distance ladder methods, is free from various calibration issues. In addition to measuring H_0, measurement of time delays between the light curves of a lensed quasar can be used to study

the microlensing variations present in the light curves, and to study the structure of the quasar (Hainline et al. 2013; Mosquera et al. 2013). However, these time delay measurements of H_0 are extremely challenging because of the need of an intensive monitoring program that offers high cadence and good-quality photometric data over a long period of time. This type of program would then be able to cope with the presence of uncorrelated variations present in the lensed quasar light curves, which can interestingly arise due to microlensing by stars in the lensing galaxy (Chang & Refsdal 1979) or for mundane reasons, such as the presence of additive flux shifts in the photometry (Tewes et al. 2013a). Moreover, the estimation of H_0 from such high-quality data is hampered by the uncertainty on lens models. Recently, using time delay measurements from high-quality optical and radio light curves, deep and high-resolution imaging observations of the lensing galaxies and lensed AGN host galaxy, and the measurement of stellar velocity dispersion of the lens galaxy to perform detailed modeling, Suyu et al. (2013) report a H_0 of $75.2^{+4.4}_{-4.2}$ km s^{-1} Mpc^{-1} through the study of two gravitational lenses namely RX J1131−1231 and CLASS B1608+656.

Another approach is to perform simple modeling of a relatively large sample of gravitational lenses with moderate-precision time delay measurements. In this way, it should be possible to obtain a precise determination of the global value of H_0, even if the H_0 measurements from individual lenses have large uncertainties. In addition, when inferring H_0 from a relatively large sample of lenses, line-of-sight effects that bias the H_0 measurements from individual lenses (see Suyu et al. 2013, Sect. 2) should tend to average out, although a residual systematic error must still remain (Hilbert et al. 2007; Fassnacht et al. 2011). A pixelized method of lens modeling is available in the literature and is also implemented in the publicly available code PixeLens (Saha & Williams 2004). Using this code, Saha et al. (2006) have found $H_0 = 72^{+8}_{-11}$ km s^{-1} Mpc^{-1} for a sample of ten time delay lenses. Performing a similar analysis on an extended sample of 18 lenses Paraficz & Hjorth (2010) obtained $H_0 = 66^{+6}_{-4}$ km s^{-1} Mpc^{-1}. Here, we present an estimate of H_0 using the pixellated modeling approach on a sample of carefully selected lensed quasars. So far, time delays have been reported for 24 gravitationally lensed quasars among the hundreds of such strongly lensed quasars known. However, the quality of the light curves and the techniques used to infer these time delays vary between systems. In this work, we apply the difference-smoothing technique, introduced in Rathna Kumar et al. (2013), to the publicly available light curves of the 24 systems in a homogeneous manner, first to cross-check the previously measured time delays and then to select a subsample of suitable lens systems to determine H_0.

The paper is organized as follows. Section 2 describes the technique used for time delay determination and introduces a recipe for creating realistic simulated light curves with known time delays; the simulated light curves are used in this work to estimate the uncertainty of each measured delay. In Sect. 3, the application of the curve-shifting procedure to the 24 systems is described. In Sect. 4, we infer H_0 from the lens-modeling of those systems that have at least one reliably measured time delay, known lens redshift, accurate astrometric data, and sufficiently simple mass distribution. We conclude in Sect. 5.

2. Time delay determination

In this section, we briefly describe the previously reported difference-smoothing technique, which contains one

modification to the original version (see Rathna Kumar et al. 2013 for details). We then introduce a recipe for simulating realistic light curves having known time delays in a plausible range around the measured delay in order to estimate its uncertainty. We also present an approach for tuning the free parameters of the difference-smoothing technique for a given dataset.

2.1. Difference-smoothing technique

A_i and B_i are the observed magnitudes constituting light curves A and B sampled at epochs t_i ($i = 1, 2, 3, ..., N$). Light curve A is selected as the reference. We shift light curve B in time with respect to light curve A by an amount τ. This shifted version B' of B is given by

$$B'_i = B_i, \tag{1}$$
$$t'_i = t_i + \tau. \tag{2}$$

We note here that we do not apply any flux shift to light curve B as in Rathna Kumar et al. (2013), since we have found that doing so considerably increases the computational time without significantly changing the results.

For any given estimate of the time delay τ, we form a difference light curve having points d_i at epochs t_i,

$$d_i(\tau) = A_i - \frac{\sum_{j=1}^{N} w_{ij} B'_j}{\sum_{j=1}^{N} w_{ij}}, \tag{3}$$

where the weights w_{ij} are given by

$$w_{ij} = \frac{1}{\sigma^2_{B_j}} e^{-(t'_j - t_i)^2 / 2\delta^2}. \tag{4}$$

The parameter δ is the decorrelation length and σ_{B_j} denotes the photometric error of the magnitude B_j. We calculate the uncertainty of each d_i as

$$\sigma_{d_i} = \sqrt{\sigma^2_{A_i} + \frac{1}{\sum_{j=1}^{N} w_{ij}}}, \tag{5}$$

where w_{ij} are given by Eq. (4).

We now smooth the difference curve d_i using a Gaussian kernel to obtain a model f_i for the differential extrinsic variability

$$f_i = \frac{\sum_{j=1}^{N} v_{ij} d_j}{\sum_{j=1}^{N} v_{ij}}, \tag{6}$$

where the weights v_{ij} are given by

$$v_{ij} = \frac{1}{\sigma^2_{d_j}} e^{-(t_j - t_i)^2 / 2s^2}. \tag{7}$$

The smoothing time scale s is another free parameter of this method. The uncertainty of each f_i is computed as

$$\sigma_{f_i} = \sqrt{\frac{1}{\sum_{j=1}^{N} v_{ij}}}. \tag{8}$$

We optimize the time delay estimate τ to minimize the residuals between the difference curve d_i and the much smoother f_i. To quantify the mismatch between d_i and f_i, we define a normalized χ^2,

$$\overline{\chi}^2 = \left[\sum_{i=1}^{N} \frac{(d_i - f_i)^2}{\sigma^2_{d_i} + \sigma^2_{f_i}} \right] / \left[\sum_{i=1}^{N} \frac{1}{\sigma^2_{d_i} + \sigma^2_{f_i}} \right], \tag{9}$$

and minimize this $\overline{\chi}^2(\tau)$ using a global optimization.

In the above description, since light curves A and B are not interchangeable, we systematically perform all computations for both permutations of A and B, and minimize the average of the two resulting values of $\overline{\chi}^2$.

2.2. Simulation of light curves

In Rathna Kumar et al. (2013), in order to estimate the uncertainty of the time delay measured using the difference-smoothing technique, we made use of realistic simulated light curves, which were created following the procedure introduced in Tewes et al. (2013a). In this work, we introduce an independent recipe for creating simulated light curves.

We infer the underlying variation $A(t)$ of the light curve A at the epoch t_i based on the magnitudes A_j for all the epochs as

$$A(t_i) = \frac{\sum_{j=1}^{N} \frac{1}{\sigma_{A_j}^2} e^{-(t_j - t_i)^2 / 2m^2} A_j}{\sum_{j=1}^{N} \frac{1}{\sigma_{A_j}^2} e^{-(t_j - t_i)^2 / 2m^2}}, \tag{10}$$

where the value of m is set to equal the mean sampling of the light curves calculated after excluding the large gaps following a 3σ rejection criterion. For those points having the nearest neighboring points on both sides separated by a value less than or equal to m, we compute the values of $(A_i - A(t_i))/\sigma_{A_i}$, the standard deviation of which is multiplied to the error bars σ_{A_i} to obtain the rescaled error bars $\hat{\sigma}_{A_i}$. We note here that the rescaling is applied for all the epochs and not just the epochs of points used in computing the rescaling factor. Similarly for the B light curves the rescaled error bars $\hat{\sigma}_{B_i}$ are obtained. This rescaling inferred from the local scatter properties of the light curves is done because the magnitudes of the original error bars may suffer from systematic underestimation or overestimation.

We merge light curves A and B by shifting the B light curve by the time delay found (Δt) and subtracting the differential extrinsic variability f_i corresponding to the delay from the A light curve. This merged light curve M_i, whose errors we denote σ_{M_i}, consists of the magnitudes $A_i - f_i$ at times t_i and having errors $\hat{\sigma}_{A_i}$ and the magnitudes B_i at times $t_i + \Delta t$ and having errors $\hat{\sigma}_{B_i}$. We now model the quasar brightness variation $M(t)$ as

$$M(t) = \frac{\sum_{j=1}^{2N} \frac{1}{\sigma_{M_j}^2} e^{-(t_j - t)^2 / 2m^2} M_j}{\sum_{j=1}^{2N} \frac{1}{\sigma_{M_j}^2} e^{-(t_j - t)^2 / 2m^2}}. \tag{11}$$

We then model the quasar brightness variation using only the A points in M_i as

$$M_A(t) = \frac{\sum_{j=1}^{N} \frac{1}{\hat{\sigma}_{A_j}^2} e^{-(t_j - t)^2 / 2m^2} (A_j - f_j)}{\sum_{j=1}^{N} \frac{1}{\hat{\sigma}_{A_j}^2} e^{-(t_j - t)^2 / 2m^2}} \tag{12}$$

and only the B points in M_i as

$$M_B(t) = \frac{\sum_{j=1}^{N} \frac{1}{\hat{\sigma}_{B_j}^2} e^{-(t_j + \Delta t - t)^2 / 2m^2} B_j}{\sum_{j=1}^{N} \frac{1}{\hat{\sigma}_{B_j}^2} e^{-(t_j + \Delta t - t)^2 / 2m^2}}. \tag{13}$$

The residual extrinsic variations present in the A and B light curves can now be calculated as

$$f_{A_i} = M_A(t_i) - M(t_i) \tag{14}$$

and

$$f_{B_i} = M_B(t_i) - M(t_i). \tag{15}$$

We can now simulate light curves A_i^{simu} and B_i^{simu} having a time delay of $\Delta t + dt$ between them by sampling $M(t)$ at appropriate epochs and adding terms for extrinsic variations and noise,

$$A_i^{\text{simu}} = M\left(t_i - \frac{dt}{2}\right) + f_i + f_{A_i} + N^*(0,1)\hat{\sigma}_{A_i} \tag{16}$$

and

$$B_i^{\text{simu}} = M\left(t_i + \Delta t + \frac{dt}{2}\right) + f_{B_i} + N^*(0,1)\hat{\sigma}_{B_i}, \tag{17}$$

where $N^*(0,1)$ is a random variate drawn from a normal distribution having mean 0 and variance 1. These simulated light curves are then assigned the times t_i and the error bars σ_{A_i} and σ_{B_i} for the A and B light curves, respectively. Including the terms f_{A_i} and f_{B_i} in the calculation of A_i^{simu} and B_i^{simu}, respectively, ensures that our simulated light curves contain extrinsic variability on all time scales, just as in the real light curves.

Here again in the above description, since light curves A and B are not interchangeable, we systematically perform all computations for both permutations of A and B, and average the corresponding values of A_i^{simu} and B_i^{simu}, before adding the noise terms.

2.3. Choice of free parameters

The value chosen for the decorrelation length δ needs to be equivalent to the temporal sampling of the light curves. In this work, we set δ equal to m, the mean sampling of the light curves calculated after excluding the large gaps following a 3σ rejection criterion.

The value chosen for the smoothing time scale s needs to be significantly larger than δ. In this work, its value is optimized such that the larger of the maximum absolute values of $\frac{f_{A_i}}{\hat{\sigma}_{A_i}}$ and $\frac{f_{B_i}}{\hat{\sigma}_{B_i}}$, which quantify the residual extrinsic variations in units of photometric noise for the A and B light curves respectively, is equal to 2. This choice ensures that the value of s is small enough to adequately model the extrinsic variations, so that the extreme values of residual extrinsic variations are not significantly larger than the noise in the data.

Again as in the above description, because light curves A and B are not interchangeable, we systematically perform all the computations for both permutations of A and B, and average the corresponding maximum absolute values.

2.4. Estimation of uncertainty

We create 200 simulated light curves having a true delay of Δt between them. The difference-smoothing technique is applied on each of them to obtain 200 delay values. The standard deviation of the 200 delay values gives us the random error, and the systematic error is obtained by the difference between the mean of the 200 delay values and the true delay. The total error $\Delta \tau_0$ is obtained by adding the random error and the systematic error in quadrature.

However, as noted by Tewes et al. (2013a), it is important to simulate light curves that have not only the time delay Δt found, but also other time delays in a plausible range around Δt, so as to obtain a reliable estimate of the uncertainty (see also
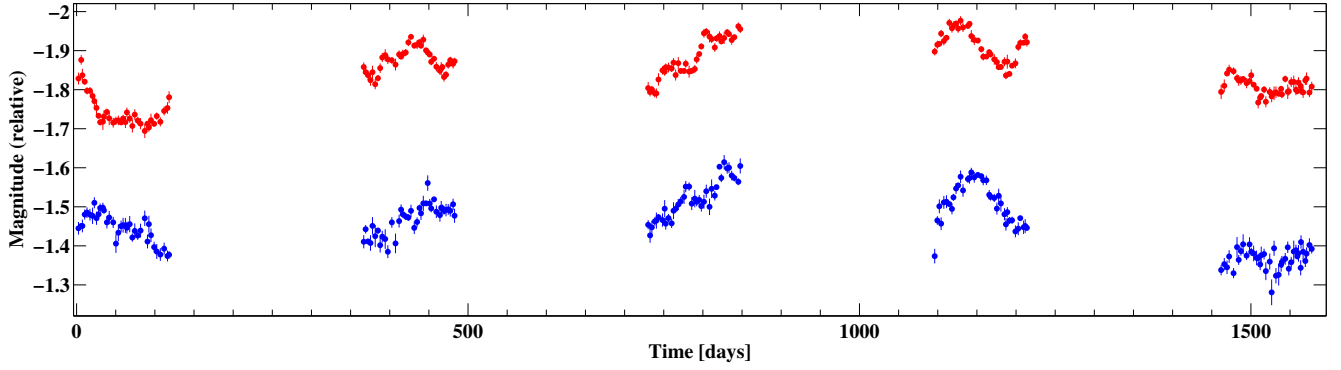
Fig. 1. Light curves from the Strong Lens Time Delay Challenge file "tdc1_rung3_quad_pair9A.txt". Light curve *A* is shown in red and light curve *B* in blue.
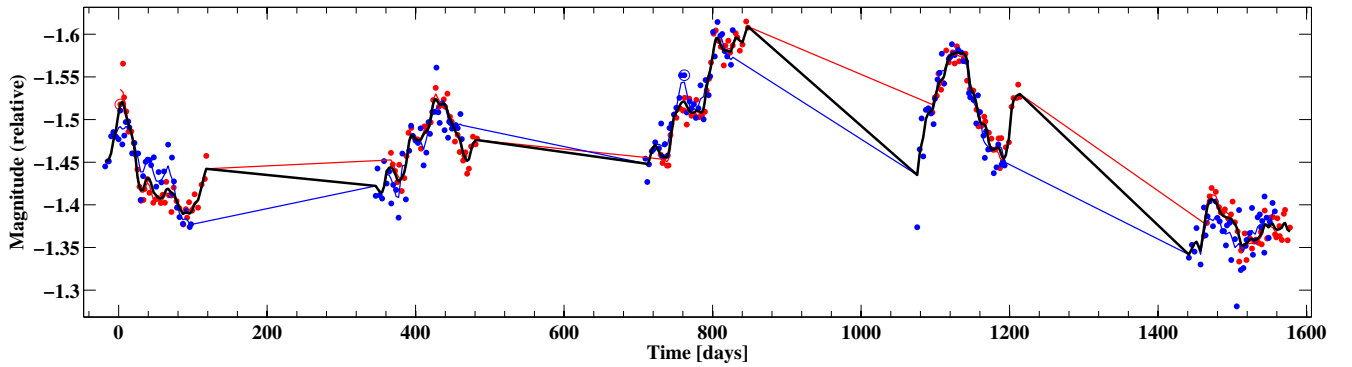
Fig. 2. Light curves *A* and *B* from Fig. 1 have been merged, with light curve *A* as reference, after shifting light curve *B* by the measured time delay of $\Delta t = -20.5$ days and subtracting the differential extrinsic variability from *A*. $M_A(t)$ sampled at the epochs t_i and $M_B(t)$ sampled at the epochs $t_i + \Delta t$ are connected by red and blue lines, respectively. $M(t)$ sampled at the epochs t_i and $t_i + \Delta t$ are connected by black lines. The optimum free parameters for this pair of light curves were found to be $\delta = 3.1$ days and $s = 139.0$ days. The magnitudes at those epochs corresponding to maximum absolute values of $\frac{f_{A_i}}{\hat{\sigma}_{A_i}}$ and $\frac{f_{B_i}}{\hat{\sigma}_{B_i}}$ have been circled. The negative value of time delay implies that light curve *A* leads light curve *B*. The magnitudes are shown without error bars for convenience of display.

Sect. 3.2 in Rathna Kumar et al. 2013). To this end, we also simulate 200 light curves for each true delay that differs from Δt by $\pm\Delta\tau_0, \pm(\Delta\tau_0 + \Delta\tau_1), ..., \pm(\Delta\tau_0 + \Delta\tau_1 + ... + \Delta\tau_{n-1})$, in each step updating the total error $\Delta\tau_n$ by adding the maximum obtained value of the random error and the maximum obtained absolute value of the systematic error in quadrature. The value of n is chosen to be the smallest integer for which

$$\Delta\tau_0 + \Delta\tau_1 + ... + \Delta\tau_{n-1} \geq 2\Delta\tau_n. \tag{18}$$

This ensures that we have simulated light curves over a range of delay values that is at least as wide as or wider than the 95.4% confidence interval implied by the stated final error $\Delta\tau_n$.

2.5. Testing the robustness of the procedure

In order to test the robustness of our procedure for estimating the time delay and its uncertainty, we made use of synthetic light curves from the TDC1 stage of the Strong Lens Time Delay Challenge[1] (Liao et al. 2015), which are arranged in five rungs having different sampling properties (see Liao et al. 2015, Table 1). We applied our procedure on a sample of 250 light curves, 50 from each rung, selected such that we were able to reliably measure time delays from them. Comparing our results with the truth files, we found that all the measured delays agreed with the true delays to within twice the estimated uncertainties,

except in one case. For the exceptional case, the discrepancy between the measured delay and the true delay was found to be 2.25σ. This is still a reasonably good level of agreement, thus demonstrating the robustness of our procedure. We note here that this property of robustness also depends on the careful choice of free parameters as presented here. For instance, setting δ equal to the mean sampling of the light curves computed without excluding the large gaps was found to lead to biased time delay measurements, which was especially noticeable for light curves having shorter seasons and larger cadence. We show some plots for the pair of TDC1 light curves corresponding to the exceptional case mentioned above in Figs. 1–3.

3. Time delays of 24 gravitationally lensed quasars

Time delays have been reported for 24 gravitationally lensed quasars. However, the quality of the data and the curve-shifting procedure followed differs from system to system. In this section, we present a homogeneous analysis of their publicly available light curves following the procedure described in the previous section, with the aim of identifying those systems that have reliable time delay measurements. In the case of systems with more than two images, we measured the time delays between all pairs of light curves. The results are summarized in Table 1. All quoted uncertainties are 1σ error bars, unless stated otherwise. Additional information on some systems listed in Table 1 and discussion on the possible reasons for our inability to reliably

---

[1] http://timedelaychallenge.org/
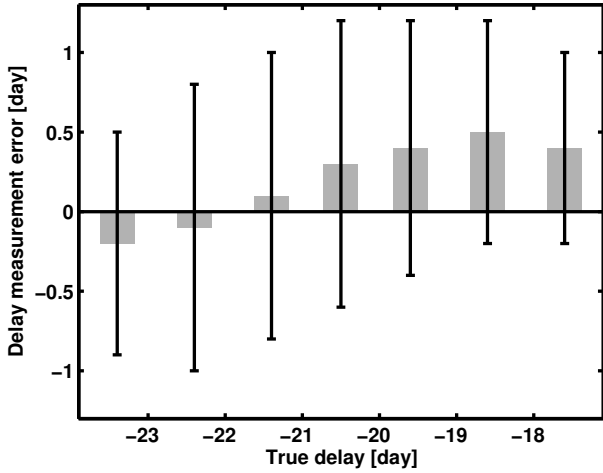
Fig. 3. Error analysis of the time delay measurement based on delay estimations on simulated light curves that mimic the light curves displayed in Fig. 1. The horizontal axis corresponds to the value of the true time delay used in these simulated light curves. The gray colored rods and 1σ error bars show the systematic biases and random errors, respectively. Our measured time delay of $\Delta t = -20.5 \pm 1.0$ days is discrepant with the true time delay of 22.75 days listed in the TDC1 truth files at the level of 2.25σ. The difference in sign of time delay is simply a matter of convention.

measure some of the time delays follow. For all the other systems, our time delay measurements agree with the previously reported values to within 2σ.

- *Q0142−100 (UM673)*: we were unable to make a reliable time delay measurement using the light curves presented in Koptelova et al. (2012). This is not surprising given that the light curves are characterized by large seasonal gaps and there are no clear variability features that could be matched between the *A* and *B* light curves.
- *JVAS B0218+357*: from 8 GHz and 15 GHz VLA observations reported by Cohen et al. (2000), we measured time delays of 10.4 ± 1.0 days and 11.4 ± 1.5 days, respectively. Taking the weighted average of the two results, we find the time delay to be 10.7 ± 0.8 days. We note here that Biggs et al. (1999) monitored this system using VLA during the same period as Cohen et al. (2000) at the same two frequencies and report a time delay of 10.5 ± 0.4 days (95% CI).
- *HE 0435−1223*: we made use of the light curves presented in Courbin et al. (2011) spanning seven seasons using data from *Euler*, *Mercator*, Maidanak, and SMARTS and the light curves presented in Blackburne et al. (2014) spanning eight seasons using data from SMARTS. The SMARTS data used by Courbin et al. (2011) is the same as the first two seasons of data presented in Blackburne et al. (2014). Hence we excluded the SMARTS data points from the light curves of Courbin et al. (2011) to make it independent of the light curves of Blackburne et al. (2014). Owing to the differences in the approaches followed by these two teams of authors to derive photometry and also the photometric uncertainties, we avoided merging the two datasets. Our time delay measurements listed in Table 1 are the weighted averages of the time delays measured from the two independent sets of light curves. The reported time delay values in Table 1 are from Courbin et al. (2011). The best-fit time delay values reported without uncertainties by Blackburne et al. (2014) are consistent with the values of Courbin et al. (2011) to within 1σ. In Table 2, we present our measurements of the time delays of

HE 0435−1223 from the two independent sets of light curves and the resulting weighted averages. For each pair of quasar images, we see that the time delays measured from the two datasets agree to within 2σ.

- *SBS 0909+532*: for our analysis, we used only the *r*-band data points obtained using the Liverpool Robotic Telescope between 2005 January and 2007 January presented in Goicoechea et al. (2008) and Hainline et al. (2013), based on homogeneity and sampling considerations.
- *RX J0911.4+0551*: we used the light curves presented in Hjorth et al. (2002), which were made publicly available by Paraficz et al. (2006).
- *FBQ 0951+2635*: we used the light curves presented in Jakobsson et al. (2005), which were made publicly available by Paraficz et al. (2006).
- *Q0957+561*: from the *r*-band and *g*-band light curves presented in Shalyapin et al. (2012), we measured time delays of 420.6 ± 1.8 days and 419.2 ± 2.2 days, respectively. Taking the weighted average of the two results, we find the time delay to be 420.0 ± 1.4 days. The reported delay listed is the weighted average of the two delays found by Shalyapin et al. (2012).
- *RX J1131−1231*: Tewes et al. (2013b) measured time delays between all pairs of light curves using three different numerical techniques. The time delay value listed in the table for each pair of light curves is for the technique that resulted in the smallest uncertainty.
- *H1413+117*: the light curves presented in Goicoechea & Shalyapin (2010) span less than one season and display poor variability. Hence our time delay measurements for the pairs *AB*, *AC*, and *AD* although in good agreement with the reported values, are of low precision and we could not reliably measure time delays for the pairs *BC* and *BD*.
- *CLASS B1600+434*: from both the optical light curves presented in Burud et al. (2000; and made publicly available by Paraficz et al. 2006) and the radio light curves presented in Koopmans et al. (2000), we were unable to make a reliable time delay measurement. Although the optical light curves show good variability, they suffer from poor sampling and thus exclude the possibility of convincingly matching the variability features between light curves *A* and *B*. The radio light curves spanning one season is well sampled; however, light curve *A* displays short time scale fluctuations that are not seen in light curve *B*, thus making it difficult to measure the time delay unambiguously.
- *HE 2149−2745*: we used the light curves presented in Burud et al. (2002a), which were made publicly available by Paraficz et al. (2006).

4. H_0 from pixellated modeling of ten gravitational lenses

Of the 24 systems analyzed in the last section, 14 of them had light curves of sufficiently good quality to enable the measurement of at least one time delay between the images, adjacent to each other in terms of arrival-time order, to a precision of better than 20% (which corresponds to a 5σ detection of time delay). The ten systems which did not satisfy this criterion are Q0142−100 (UM673), FBQ 0951+2635, PG 1115+080, H1413+117, JVAS B1422+231, CLASS B1600+434, SDSS J1650+4251, PKS 1830−211, HE 2149−2745, and HS 2209+1914.

Of the 14 remaining systems, we did not model the mass distribution for four of them for the following reasons.

Table 1. Summary of time delay measurements.

Object (reference for data)	Wavebands	Time delay	Reported value[a] (days)	Our measurement[a] (days)
Q0142−100 (Koptelova et al. 2012)	R	Δt_{AB}	89 ± 11	?
JVAS B0218+357 (Cohen et al. 2000)	8 GHz, 15 GHz	Δt_{AB}	$10.1^{+1.5}_{-1.6}$ (95% CI)	10.7 ± 0.8
HE 0435−1223 (Courbin et al. 2011; Blackburne et al. 2014)	R	Δt_{AB}	8.4 ± 2.1	9.8 ± 1.1
		Δt_{AC}	0.6 ± 2.3	3.1 ± 2.2
		Δt_{AD}	14.9 ± 2.1	13.7 ± 1.0
		Δt_{BC}	-7.8 ± 0.8	-8.0 ± 1.0
		Δt_{BD}	6.5 ± 0.7	6.2 ± 1.5
		Δt_{CD}	14.3 ± 0.8	13.6 ± 0.8
SBS 0909+532 (Goicoechea et al. 2008; Hainline et al. 2013)	r	Δt_{AB}	-50^{+2}_{-4}	-45.9 ± 3.1
RX J0911.4+0551 (Hjorth et al. 2002)	I	$\Delta t_{(A1+A2+A3)B}$	-146 ± 8 (2σ)	-141.9 ± 12.3
FBQ 0951+2635 (Jakobsson et al. 2005)	R	Δt_{AB}	16 ± 2	7.8 ± 14.0
Q0957+561 (Shalyapin et al. 2012)	r, g	Δt_{AB}	417.4 ± 0.9	420.0 ± 1.4
SDSS J1001+5027 (Rathna Kumar et al. 2013)	R	Δt_{AB}	119.3 ± 3.3	119.7 ± 1.8
SDSS J1004+4112 (Fohlmeister et al. 2007; Fohlmeister et al. 2008)	R, r	Δt_{AB}	-40.6 ± 1.8	-37.2 ± 3.1
		Δt_{AC}	-821.6 ± 2.1	-822.5 ± 7.4
		Δt_{BC}		-777.1 ± 9.2
SDSS J1029+2623 (Fohlmeister et al. 2013)	r	$\Delta t_{A(B+C)}$	744 ± 10 (90% CI)	734.3 ± 3.8
HE 1104−1805 (Poindexter et al. 2007)	R, V	Δt_{AB}	$-152.2^{+2.8}_{-3.0}$	-157.1 ± 3.6
PG 1115+080 (Tsvetkova et al. 2010)	R	$\Delta t_{(A1+A2)B}$	$4.4^{+3.2}_{-2.5}$	8.7 ± 3.6
		$\Delta t_{(A1+A2)C}$	$-12^{+2.5}_{-2.0}$	-12.1 ± 3.6
		Δt_{BC}	$-16.4^{+3.5}_{-2.5}$	-23.9 ± 5.7
RX J1131−1231 (Tewes et al. 2013b)	R	Δt_{AB}	0.7 ± 1.0	0.0 ± 0.6
		Δt_{AC}	0.0 ± 1.3	-1.1 ± 0.8
		Δt_{AD}	90.6 ± 1.4	91.7 ± 0.7
		Δt_{BC}	-0.7 ± 1.5	-1.4 ± 1.6
		Δt_{BD}	91.4 ± 1.2	92.4 ± 1.4
		Δt_{CD}	91.7 ± 1.5	91.3 ± 1.3
SDSS J1206+4332 (Eulaers et al. 2013)	R	Δt_{AB}	111.3 ± 3	110.3 ± 1.9
H1413+117 (Goicoechea & Shalyapin 2010)	r	Δt_{AB}	-17 ± 3	-14.3 ± 5.5
		Δt_{AC}	-20 ± 4	-19.9 ± 10.9
		Δt_{AD}	23 ± 4	24.0 ± 6.8
		Δt_{BC}		?
		Δt_{BD}		?
		Δt_{CD}		28.6 ± 9.4
JVAS B1422+231 (Patnaik & Narasimha 2001)	15 GHz	Δt_{AB}	-1.5 ± 1.4	1.1 ± 2.1
		Δt_{AC}	7.6 ± 2.5	-0.4 ± 3.0
		Δt_{BC}	8.2 ± 2.0	-0.4 ± 3.2
SBS 1520+530 (Burud et al. 2002b)	R	Δt_{AB}	130 ± 3	124.2 ± 8.1
CLASS B1600+434 (Burud et al. 2000)	I	Δt_{AB}	51 ± 4 (95% CI)	?
CLASS B1600+434 (Koopmans et al. 2000)	8.5 GHz	Δt_{AB}	47^{+5}_{-6}	?
CLASS B1608+656 (Fassnacht et al. 1999; Fassnacht et al. 2002)	8.5 GHz	Δt_{AB}	$-31.5^{+2.0}_{-1.0}$	-32.4 ± 3.0
		Δt_{AC}		2.3 ± 1.2
		Δt_{AD}		45.7 ± 0.9
		Δt_{BC}	$36.0^{+1.5}_{-1.5}$	37.1 ± 1.9
		Δt_{BD}	$77.0^{+2.0}_{-1.0}$	77.6 ± 3.5
		Δt_{CD}		41.3 ± 1.6
SDSS J1650+4251 (Vuissoz et al. 2007)	R	Δt_{AB}	49.5 ± 1.9	59.2 ± 15.9
PKS 1830−211 (Lovell et al. 1998)	8.6 GHz	Δt_{AB}	26^{+4}_{-5}	28.6 ± 8.0
WFI J2033−4723 (Vuissoz et al. 2008)	R	Δt_{AB}	-35.5 ± 1.4	-37.6 ± 2.1
		Δt_{AC}		23.6 ± 2.5
		Δt_{BC}	$62.6^{+4.1}_{-2.3}$	65.4 ± 4.3
HE 2149−2745 (Burud et al. 2002a)	V	Δt_{AB}	103 ± 12	72.6 ± 17.0
HS 2209+1914 (Eulaers et al. 2013)	R	Δt_{AB}	-20.0 ± 5	-22.9 ± 5.3

Notes. [a] A negative value of time delay implies that the arrival-time order is the reverse of what is implied in the subscript to Δt.

Table 2. Our measurements of the time delays of HE 0435−1223 from two independent datasets.

Time delay	Courbin et al. (2011)[a] (days)	Blackburne et al. (2014) (days)	Weighted average (days)
Δt_{AB}	8.4 ± 1.4	12.3 ± 1.9	9.8 ± 1.1
Δt_{AC}	3.6 ± 3.4	2.7 ± 2.9	3.1 ± 2.2
Δt_{AD}	13.1 ± 1.1	15.8 ± 2.1	13.7 ± 1.0
Δt_{BC}	−8.3 ± 1.5	−7.7 ± 1.4	−8.0 ± 1.0
Δt_{BD}	5.7 ± 1.7	7.9 ± 3.2	6.2 ± 1.5
Δt_{CD}	13.0 ± 1.1	14.1 ± 1.1	13.6 ± 0.8

Notes. [a] The SMARTS data points were excluded from the light curves of Courbin et al. (2011) so that the measured time delay values were independent of those measured from the SMARTS monitoring light curves of Blackburne et al. (2014; see discussion in Sect. 3).

SDSS J1001+5027 and SDSS J1206+4332 do not have accurate astrometric data measured from *Hubble* Space Telescope (HST) images or ground-based imaging with adaptive optics. Although the astrometry of JVAS B0218+357, which has a small image separation of 0.33″, has been measured from HST images by Sluse et al. (2012), the authors warn about possibly large systematic errors in the published astrometry. SDSS J1029+2623 is a three-image cluster lens with highly complex mass distribution (see Oguri et al. 2013) and hence not amenable to lens-modeling following the simplistic approach described below.

To perform mass-modeling of the remaining ten systems – HE 0435−1223, SBS 0909+532, RX J0911.4+0551, Q0957+561, SDSS J1004+4112, HE 1104−1805, RX J1131−1231, SBS 1520+530, CLASS B1608+656 and WFI J2033−4723 – to infer H_0, we used the publicly available PixeLens[2] code (Saha & Williams 2004), which builds an ensemble of pixellated mass maps compatible with the input data for a given system, which is comprised of the redshifts of the quasar and the lensing galaxy, the arrival-time order of the images, their astrometry relative to the center of the main lensing galaxy, and the known time delays between the images adjacent to each other in terms of arrival-time order. In case of quadruple lenses in which only some of the time delays are known, it is still possible to guess the arrival-time order of the images by following certain simple rules (see Saha & Williams 2003).

We model all lenses, except SDSS J1004+4112, such that their mass profiles have inversion symmetry about the lens center, including any companion galaxy to the main lensing galaxy as a point mass. The lensing cluster in SDSS J1004+4112 consists of several galaxies besides the main lensing galaxy (see Inada et al. 2005) and hence was modeled without assuming inversion symmetry about the lens center.

PixeLens builds models such that their projected density profiles are steeper than $|\theta|^{-\gamma_{\min}}$, where $|\theta|$ is the distance from the center of the lens in angular units, the default value of $\gamma_{\min}$ being 0.5. This is based on the observation that the total density distribution in the central regions of elliptical galaxies is close to isothermal (i.e., r^{-2}) and also the observation that the total density in the center of our Galaxy scales is $r^{-1.75}$ (see Saha & Williams 2004, Sect. 2.2 and references therein). The profiles r^{-2} and $r^{-1.75}$ correspond to projected density profiles of $|\theta|^{-1}$ and $|\theta|^{-0.75}$, respectively, in the special case of spherical symmetry. In this work, we relax the restriction of $\gamma_{\min} = 0.5$ and set $\gamma_{\min} = 0$ for those lenses in our sample in which the largest angular separation between the images is greater than 3″. The lenses in our sample that satisfy this criterion are RX J0911.4+0551, Q0957+561, SDSS J1004+4112, HE 1104−1805, and RX J1131−1231. A large image separation

implies that there is significant lensing action from the cluster of which the main lensing galaxy is part, in which case the projected density profile can be shallower than $|\theta|^{-0.5}$.

For each system, we build an ensemble of 100 models, corresponding to 100 values of H_0. The mean of the 100 values gives the best estimate of H_0, the uncertainty of which is the standard deviation of the 100 values. This uncertainty includes only the uncertainty in the mass model. PixeLens assumes that the uncertainty in the input priors to be negligibly small, which is a reasonable assumption for the redshifts, if they are spectroscopically measured, and astrometry, if measured from HST or ground-based adaptive optics imaging. However, the measured time delays have finite uncertainties, which need to be propagated into the uncertainty of the estimated H_0. We do this by remodeling each system after perturbing the time delay by its 1σ uncertainty and noticing the deviation of the resulting value of H_0 from the original value. For high-precision time delays, the deviation in H_0 was found to be the same whether the delays were perturbed upward or downward. In general, the deviation in H_0 was found to be slightly larger when the delays were perturbed downward than when they were perturbed upward. Hence in this work, to get a conservative estimate of the contribution of the time delay uncertainty to the uncertainty in H_0, we decrease the time delay by its 1σ uncertainty and find the resulting increase in H_0. This uncertainty in H_0 resulting from the time delay uncertainty is added in quadrature to the uncertainty in H_0 resulting from mass modeling to find the total uncertainty. In the case of quadruple lenses where more than one time delay is known, we perturb each delay individually while leaving the other delays unchanged to infer its uncertainty contribution. The uncertainty contribution from each independent time delay is then added in quadrature to the uncertainty in H_0 resulting from the uncertainty in the mass model to find the total uncertainty.

In order to include the effects of external shear, an approximate direction of the shear axis needs to be specified and PixeLens will search for solutions within $45°$ of the specified direction. Since there is no simple rule to guess the direction of the external shear for a given system, for each system, we repeated the modeling specifying the approximate direction of the shear axis as $90°$, $45°$, $0°$, and $-45°$ (in this instance, specifying θ and $\theta+180°$ are equivalent). We thus obtain four estimates of H_0 and their uncertainties. In each case, we propagate the uncertainty contributions from the known time delays to the uncertainty in H_0, as discussed previously. The final estimate of H_0 and its uncertainty are found using maximum likelihood analysis, optimizing their values so as to maximize the joint posterior probability of these two parameters for the sample consisting of the four H_0 values and their uncertainties (see Barnabè et al. 2011, Eq. (7)). In optimizing the value of the uncertainty, we

---

[2] http://www.physik.uzh.ch/~psaha/lens/pixelens.php

Table 3. Summary of input data to PixeLens and resulting H_0 estimates.

| Object	Redshifts	Image[a] / P.M.[b]	ΔRA[c] (″)	ΔDec[c] (″)	Delay[d] (days)	H_0[e] (km s^{-1} Mpc^{-1})	References[f]
HE 0435−1223	$z_l = 0.4546$	A	1.1706	0.5665		64.1 ± 21.3	Morgan et al. (2005)
	$z_s = 1.689$	C	−1.2958	−0.0357		(64.1 ± 19.4)	Wisotzki et al. (2002)
		B	−0.3037	1.1183	8.0 ± 1.0		Courbin et al. (2011)
		D	0.2328	−1.0495			
SBS 0909+532	$z_l = 0.830$	B	0.5228	−0.4423		63.9 ± 17.3	Lubin et al. (2000)
	$z_s = 1.377$	A	−0.4640	0.0550	45.9 ± 3.1	(63.9 ± 16.8)	Kochanek et al. (1997)
							Sluse et al. (2012)
RX J0911.4+0551	$z_l = 0.769$	B	−2.2662	0.2904		80.0 ± 31.8	Kneib et al. (2000)
	$z_s = 2.800$	A2	0.9630	−0.0951	141.9 ± 12.3	(80.0 ± 31.0)	Bade et al. (1997)
		A1	0.7019	−0.5020			Sluse et al. (2012)
		A3	0.6861	0.4555			
		P.M.	−0.7582	0.6658			
Q0957+561	$z_l = 0.361$	A	1.408	5.034		96.9 ± 31.3	Walsh et al. (1979)
	$z_s = 1.41$	B	0.182	−1.018	420.0 ± 1.4	(96.9 ± 31.3)	Fadely et al. (2010)
SDSS J1004+4112	$z_l = 0.68$	C	3.925	−8.901		89.9 ± 28.3	Oguri et al. (2004)
	$z_s = 1.734$	B	−8.431	−0.877	777.1 ± 9.2	(89.9 ± 28.1)	Inada et al. (2003)
		A	−7.114	−4.409	37.2 ± 3.1		Inada et al. (2005)
		D	1.285	5.298			
HE 1104−1805	$z_l = 0.729$	B	1.9289	−0.8242		104.0 ± 53.0	Lidman et al. (2000)
	$z_s = 2.319$	A	−0.9731	0.5120	157.1 ± 3.6	(104.0 ± 52.9)	Smette et al. (1995)
							Sluse et al. (2012)
RX J1131−1231	$z_l = 0.295$	C	−1.460	−1.632		71.9 ± 25.6	Sluse et al. (2003)
	$z_s = 0.658$	B	−2.076	0.662		(71.9 ± 25.6)	Suyu et al. (2013)
		A	−2.037	−0.520			
		D	1.074	0.356	91.7 ± 0.7		
		P.M.	−0.097	0.614			
SBS 1520+530	$z_l = 0.761$	A	−1.1395	0.3834		59.0 ± 15.8	Auger et al. (2008)
	$z_s = 1.855$	B	0.2879	−0.2691	124.2 ± 8.1	(59.0 ± 15.3)	Chavushyan et al. (1997)
							Sluse et al. (2012)
CLASS B1608+656	$z_l = 0.6304$	B	1.2025	−0.8931		58.7 ± 11.0	Myers et al. (1995)
	$z_s = 1.394$	A	0.4561	1.0647	32.4 ± 3.0	(58.7 ± 10.8)	Fassnacht et al. (1996)
		C	1.2044	0.6182			Sluse et al. (2012)
		D	−0.6620	−0.1880	41.3 ± 1.6		
		P.M.	0.7382	0.1288			
WFI J2033−4723	$z_l = 0.661$	B	1.4388	−0.3113		73.7 ± 12.8	Eigenbrod et al. (2006)
	$z_s = 1.66$	A1	−0.7558	0.9488	37.6 ± 2.1	(73.3 ± 11.6)	Morgan et al. (2004)
		A2	−0.0421	1.0643			Vuissoz et al. (2008)
		C	−0.6740	−0.5891	23.6 ± 2.5		
Combined						68.1 ± 5.9 (67.9 ± 5.6)	

Notes. [a] The QSO images are listed in arrival-time order. [b] "P.M." is the abbreviation for point mass and refers to secondary lensing galaxies. [c] The astrometry of the QSO images and point masses are specified with respect to the center of the main lensing galaxy. [d] The time delay of a given image is listed (if measured to a precision better than 20%) with respect to the previous image in terms of arrival-time order. [e] In parentheses we provide the H_0 estimates and their uncertainties without propagating the uncertainties in time delays. [f] The references are listed for measurements of lens redshift (z_l), source redshift (z_s), and astrometry.

choose the minimum limit to be the smallest of the four uncertainties. We note here that for the system HE 1104−1805, the choices of the approximate direction of the shear axis of 90° and −45° were found to lead to unphysical models involving negative values in the mass pixels. Hence for this system, the maximum likelihood analysis was carried out using only the two H_0 values resulting for the approximate shear directions of 45° and 0°.

The input priors for each system and the resulting H_0 estimates are summarized in Table 3. In Fig. 4 we plot the H_0 estimates from the ten lenses, all of which are seen to agree with each other within their error bars. To combine the ten independent estimates into a best estimate of H_0, we again employ maximum likelihood analysis, as described above. However, in this

case, in optimizing the value of the uncertainty of the best estimate of H_0, the minimum limit is chosen to be the uncertainty of the weighted average of the ten values. We infer a value of H_0 of 68.1 ± 5.9 km s^{-1} Mpc^{-1} (1σ uncertainty, 8.7% precision) for a spatially flat universe having $\Omega_m = 0.3$ and $\Omega_\Lambda = 0.7$. The reason for employing maximum likelihood analysis in this case, rather than taking a simple weighted average is to detect the presence of any unmodeled uncertainties. However, as can be seen from Fig. 4, the H_0 estimates from the individual systems all agree with each other within their error bars and hence the H_0 value inferred above through maximum likelihood analysis is only marginally different from the weighted average. For the source and lens redshifts of the current sample, we find the H_0 estimate to decrease by 7.1% for the Einstein-de Sitter universe
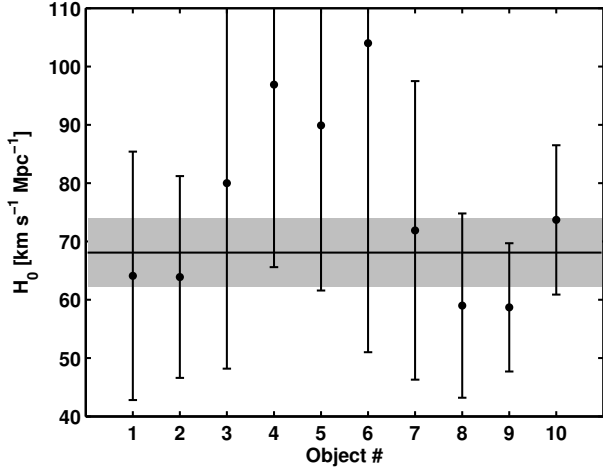
Fig. 4. H_0 estimates and their 1σ uncertainties for the ten gravitational lenses – *(1)* HE 0435−1223; *(2)* SBS 0909+532; *(3)* RX J0911.4+0551; *(4)* Q0957+561; *(5)* SDSS J1004+4112; *(6)* HE 1104−1805; *(7)* RX J1131−1231; *(8)* SBS 1520+530; *(9)* CLASS B1608+656; and *(10)* WFI J2033−4723. The best estimate of H_0 and its 1σ confidence interval, inferred through maximum-likelihood analysis, are represented by the horizontal line and the gray shaded region, respectively.

($\Omega_m = 1.0$ and $\Omega_\Lambda = 0.0$) and increase by 2.3% for an open universe having $\Omega_m = 0.3$ and $\Omega_\Lambda = 0.0$, thus illustrating the low level of dependence of the inferred value of H_0 on the precise values of Ω_m and Ω_Λ. In Table 3, we also list the H_0 estimates obtained without propagating the time delay uncertainties. We see that the dominant contribution to uncertainty in H_0 results from the uncertainty in the mass model.

5. Conclusion

We have presented a homogeneous curve-shifting analysis of the light curves of 24 gravitationally lensed quasars for which time delays have been reported in the literature so far. Time delays were measured using the difference-smoothing technique and their uncertainties were estimated using realistic simulated light curves; a recipe for creating these light curves with known time delays in a plausible range around the measured delay was introduced in this work. We identified 14 systems to have light curves of sufficiently good quality to enable the measurement of at least one time delay between the images, adjacent to each other in terms of arrival-time order, to a precision of better than 20% (including systematic errors). Of these 14 systems, we performed pixellated mass modeling using the publicly available PixeLens software for ten of them, which have known lens redshifts, accurate astrometric information, and sufficiently simple mass distributions, to infer the value of H_0 to be 68.1 ± 5.9 km s^{-1} Mpc^{-1} (1σ uncertainty, 8.7% precision) for a spatially flat universe having $\Omega_m = 0.3$ and $\Omega_\Lambda = 0.7$. We note here that we have followed a relatively simple lens modeling approach to constrain H_0 and our analysis does not account for biases resulting from line-of-sight effects.

Our measurement closely matches a recent estimate of $H_0 = 69.0 \pm 6$ (stat.) ± 4 (syst.) km s^{-1} Mpc^{-1} found by Sereno & Paraficz (2014) using a method based on free-form modeling of 18 gravitational lens systems. Our value is also consistent with the recent measurements of H_0 by Riess et al. (2011), Freedman et al. (2012) and Suyu et al. (2013); however, it has lower precision. Increasing the number of lenses with good-quality light curves, accurate astrometry, and known lens redshift from the

current ten used in this study can bring down the uncertainty in H_0.

In the future such high-precision time delays will become available from projects such as COSMOGRAIL (Tewes et al. 2012) involving dedicated medium-sized telescopes. In addition, the next generation of cosmic surveys such as the Dark Energy Survey (DES), the Large Synoptic Survey Telescope (LSST; Ivezic et al. 2008), and the Euclid mission will detect a large sample of lenses, and time delays might be available for a large fraction of them, consequently enabling measurement of H_0 to an accuracy better than 2%. Furthermore, detection of gravitational wave signals from short gamma-ray bursts associated with neutron star binary mergers in the coming decade could constrain H_0 to better than 1% (Nissanke et al. 2013).

References

Auger, M. W., Fassnacht, C. D., Wong, K. C., et al. 2008, ApJ, 673, 778
Bade, N., Siebert, J., Lopez, S., Voges, W., & Reimers, D. 1997, A&A, 317, L13
Barnabè, M., Czoske, O., Koopmans, L. V. E., Treu, T., & Bolton, A. S. 2011, MNRAS, 415, 2215
Biggs, A. D., Browne, I. W. A., Helbig, P., et al. 1999, MNRAS, 304, 349
Blackburne, J. A., Kochanek, C. S., Chen, B., Dai, X., & Chartas, G. 2014, ApJ, 789, 125
Braatz, J., Reid, M., Kuo, C.-Y., et al. 2013, in IAU Symp. 289, ed. R. de Grijs, 255
Burud, I., Hjorth, J., Jaunsen, A. O., et al. 2000, ApJ, 544, 117
Burud, I., Courbin, F., Magain, P., et al. 2002a, A&A, 383, 71
Burud, I., Hjorth, J., Courbin, F., et al. 2002b, A&A, 391, 481
Chang, K., & Refsdal, S. 1979, Nature, 282, 561
Chavushyan, V. H., Vlasyuk, V. V., Stepanian, J. A., & Erastova, L. K. 1997, A&A, 318, L67
Cohen, A. S., Hewitt, J. N., Moore, C. B., & Haarsma, D. B. 2000, ApJ, 545, 578
Courbin, F., Chantry, V., Revaz, Y., et al. 2011, A&A, 536, A53
Eigenbrod, A., Courbin, F., Meylan, G., Vuissoz, C., & Magain, P. 2006, A&A, 451, 759
Eulaers, E., Tewes, M., Magain, P., et al. 2013, A&A, 553, A121
Fadely, R., Keeton, C. R., Nakajima, R., & Bernstein, G. M. 2010, ApJ, 711, 246
Fassnacht, C. D., Womble, D. S., Neugebauer, G., et al. 1996, ApJ, 460, L103
Fassnacht, C. D., Pearson, T. J., Readhead, A. C. S., et al. 1999, ApJ, 527, 498
Fassnacht, C. D., Xanthopoulos, E., Koopmans, L. V. E., & Rusin, D. 2002, ApJ, 581, 823
Fassnacht, C. D., Koopmans, L. V. E., & Wong, K. C. 2011, MNRAS, 410, 2167
Fohlmeister, J., Kochanek, C. S., Falco, E. E., et al. 2007, ApJ, 662, 62
Fohlmeister, J., Kochanek, C. S., Falco, E. E., Morgan, C. W., & Wambsganss, J. 2008, ApJ, 676, 761
Fohlmeister, J., Kochanek, C. S., Falco, E. E., et al. 2013, ApJ, 764, 186
Freedman, W. L., & Madore, B. F. 2010, ARA&A, 48, 673
Freedman, W. L., Madore, B. F., Gibson, B. K., et al. 2001, ApJ, 553, 47
Freedman, W. L., Madore, B. F., Scowcroft, V., et al. 2012, ApJ, 758, 24
Goicoechea, L. J., & Shalyapin, V. N. 2010, ApJ, 708, 995
Goicoechea, L. J., Shalyapin, V. N., Koptelova, E., et al. 2008, New Astron., 13, 182
Hainline, L. J., Morgan, C. W., MacLeod, C. L., et al. 2013, ApJ, 774, 69
Hilbert, S., White, S. D. M., Hartlap, J., & Schneider, P. 2007, MNRAS, 382, 121
Hinshaw, G., Larson, D., Komatsu, E., et al. 2013, ApJS, 208, 19
Hjorth, J., Burud, I., Jaunsen, A. O., et al. 2002, ApJ, 572, L11
Inada, N., Oguri, M., Pindor, B., et al. 2003, Nature, 426, 810
Inada, N., Oguri, M., Keeton, C. R., et al. 2005, PASJ, 57, L7
Ivezic, Z., Tyson, J. A., Acosta, E., et al. 2008 [arXiv:0805.2366]
Jakobsson, P., Hjorth, J., Burud, I., et al. 2005, A&A, 431, 103

Kneib, J.-P., Cohen, J. G., & Hjorth, J. 2000, ApJ, 544, L35
Kochanek, C. S., Falco, E. E., Schild, R., et al. 1997, ApJ, 479, 678
Koopmans, L. V. E., de Bruyn, A. G., Xanthopoulos, E., & Fassnacht, C. D. 2000, A&A, 356, 391
Koptelova, E., Chen, W. P., Chiueh, T., et al. 2012, A&A, 544, A51
Liao, K., Treu, T., Marshall, P., et al. 2015, ApJ, 800, 11
Lidman, C., Courbin, F., Kneib, J.-P., et al. 2000, A&A, 364, L62
Lovell, J. E. J., Jauncey, D. L., Reynolds, J. E., et al. 1998, ApJ, 508, L51
Lubin, L. M., Fassnacht, C. D., Readhead, A. C. S., Blandford, R. D., & Kundić, T. 2000, AJ, 119, 451
Morgan, N. D., Caldwell, J. A. R., Schechter, P. L., et al. 2004, AJ, 127, 2617
Morgan, N. D., Kochanek, C. S., Pevunova, O., & Schechter, P. L. 2005, AJ, 129, 2531
Mosquera, A. M., Kochanek, C. S., Chen, B., et al. 2013, ApJ, 769, 53
Myers, S. T., Fassnacht, C. D., Djorgovski, S. G., et al. 1995, ApJ, 447, L5
Nissanke, S., Holz, D. E., Dalal, N., et al. 2013 [arXiv:1307.2638]
Oguri, M., Inada, N., Keeton, C. R., et al. 2004, ApJ, 605, 78
Oguri, M., Schrabback, T., Jullo, E., et al. 2013, MNRAS, 429, 482
Paraficz, D., & Hjorth, J. 2010, ApJ, 712, 1378
Paraficz, D., Hjorth, J., Burud, I., Jakobsson, P., & Elíasdóttir, Á. 2006, A&A, 455, L1
Patnaik, A. R., & Narasimha, D. 2001, MNRAS, 326, 1403
Planck Collaboration XVI. 2014, A&A, 571, A16
Poindexter, S., Morgan, N., Kochanek, C. S., & Falco, E. E. 2007, ApJ, 660, 146
Rathna Kumar, S., Tewes, M., Stalin, C. S., et al. 2013, A&A, 557, A44
Refsdal, S. 1964, MNRAS, 128, 307
Reid, M. J., Braatz, J. A., Condon, J. J., et al. 2013, ApJ, 767, 154
Riess, A. G., Macri, L., Casertano, S., et al. 2011, ApJ, 730, 119
Saha, P., & Williams, L. L. R. 2003, AJ, 125, 2769
Saha, P., & Williams, L. L. R. 2004, AJ, 127, 2604
Saha, P., Coles, J., Macciò, A. V., & Williams, L. L. R. 2006, ApJ, 650, L17
Sandage, A., Tammann, G. A., Saha, A., et al. 2006, ApJ, 653, 843
Sereno, M., & Paraficz, D. 2014, MNRAS, 437, 600
Shalyapin, V. N., Goicoechea, L. J., & Gil-Merino, R. 2012, A&A, 540, A132
Sluse, D., Surdej, J., Claeskens, J.-F., et al. 2003, A&A, 406, L43
Sluse, D., Chantry, V., Magain, P., Courbin, F., & Meylan, G. 2012, A&A, 538, A99
Smette, A., Robertson, J. G., Shaver, P. A., et al. 1995, A&AS, 113, 199
Suyu, S. H., Auger, M. W., Hilbert, S., et al. 2013, ApJ, 766, 70
Tewes, M., Courbin, F., Meylan, G., et al. 2012, The Messenger, 150, 49
Tewes, M., Courbin, F., & Meylan, G. 2013a, A&A, 553, A120
Tewes, M., Courbin, F., Meylan, G., et al. 2013b, A&A, 556, A22
Tsvetkova, V. S., Vakulik, V. G., Shulga, V. M., et al. 2010, MNRAS, 406, 2764
Vuissoz, C., Courbin, F., Sluse, D., et al. 2007, A&A, 464, 845
Vuissoz, C., Courbin, F., Sluse, D., et al. 2008, A&A, 488, 481
Walsh, D., Carswell, R. F., & Weymann, R. J. 1979, Nature, 279, 381
Wisotzki, L., Schechter, P. L., Bradt, H. V., Heinmüller, J., & Reimers, D. 2002, A&A, 395, 17